Opsins are Phospholipid Scramblases in All Domains of Life

Zachary A. Maschmann[1,*], David E. Hardy[1], Indu Menon[2], Jenna Webb[1], Anant K. Menon[2] and Katrina T. Forest[1#]

[1]*Department of Bacteriology, University of Wisconsin–Madison, Madison, WI 53706*
[2]*Department of Biochemistry, Weill Cornell Medical College, New York, NY 10065*

#For Correspondence: Katrina T. Forest, forest@bact.wisc.edu

*ZAM current address: Department of Molecular Biology, Princeton University 08540

Running Title: Bacterial Opsins are Scramblases
Competing interests: The authors declare that no competing interests exist.

Abstract

Opsins are highly abundant retinal proteins in the membranes of photoheterotrophic bacteria. However, some microbial genomes encode an *opsin* but lack the gene for the final enzyme in retinal synthesis. To account for this paradox, we hypothesized that bacterial opsins play a role in membrane structure and/or biogenesis independent from their potential for light-driven signaling or proton pumping. After purifying actinorhodopsin from a cell-free expression system and from *E. coli* membranes upon overexpression, we demonstrated both *in vitro* and *in silico* that actinorhodopsin from *Nanopelagicus ca*. is a phospholipid scramblase, serving in its pentameric state as a retinal-independent phospholipid diffusion channel. Phospholipid headgroups move along a transbilayer path between actinorhodopsin protomers, to equilibrate lipid content in the inner and outer leaflets. Two profound activities, membrane biosynthesis and capture of light energy, are thus facilitated by one ancient bacterial polypeptide. Light-dependent activity and light-independent phospholipid scrambling are shared functions of eukaryotic, archaeal, and bacterial rhodopsins.

Importance

Cells are surrounded by membranes which concentrate metabolites and protect cellular contents. Biomembranes are bilayers, each layer made of phospholipids that orient greasy tails inward and polar groups outward. Bilayer biogenesis depends on phospholipids synthesized inside the cell reorienting from the inner to the outer membrane layer. This activity was predicted before proteins responsible for it were identified, but eventually it was

shown that rhodopsins -- 7-helix photoactive membrane proteins bound to the cofactor retinal -- carry out this activity in organisms as widely divergent as mammals and archaea. Now we conclusively demonstrate using purified proteins in laboratory membranes and computational approaches, that bacteria also employ rhodopsins as phospholipid scramblases. This work is important because it highlights a surprising commonality among bacteria, archaea and eukaryotes and because it shows that rhodopsins – ancient proteins found in the last universal common ancestor – manifest two seemingly unrelated biochemical functions in one protein.

Keywords: Membrane Biogenesis, Lipid scrambling, Photoheterotrophy, Rhodopsin, Actinorhodopsin, ActR

Wordcount: Abstract 154, Text 5086

Introduction

Living cells engage in an ongoing process of self-construction. Phospholipid bilayer membranes separate the cellular interior from exterior, concentrate cytoplasmic contents, and protect cellular components. Membrane production is needed for cell division, and as part of turnover and repair processes (1). Phospholipids are synthesized in the cytoplasmic leaflet of biogenic membranes, such as the cytoplasmic membrane of bacteria and the endoplasmic reticulum(2). Reorientation of phospholipids between leaflets, *lipid scrambling,* is necessary for uniform growth of the bilayer but occurs too slowly to support life if unassisted(3–8). Biogenesis of all extant membrane bilayers requires a solution to this problem(9, 10), and evolution of this function likely would have provided ancient protocells with strong fitness benefits. Indeed, compartmentalization to support early life may have relied on the modularity and renewability of lipid bilayers (11, 12). Living cells use a facilitated lipid diffusion channel, termed a scramblase, to catalyze transbilayer phospholipid equilibration (10, 13–16). Scramblases are thought to shield the charged phospholipid head group from the hydrophobic bilayer interior to expedite lipid scrambling (10, 13–16).

In recent years, rhodopsins—well known for their photon capture based activities—have been shown to moonlight as scramblases. Menon and colleagues used a fluorescence-based assay to show that purified bovine rhodopsin exhibits scramblase activity when reconstituted into large unilamellar vesicles (17), accounting for previous observations that lipids scramble rapidly across photoreceptor disc membranes (18, 19). Scramblase activity was shown to be ATP-independent and constitutive, occurring in the absence of light or the retinal chromophore. Subsequent work showed that an archaeal rhodopsin — bacteriorhodopsin (BR) from the archaeon *Halobacterium salinarum* — also had light-independent scramblase activity (20). This functional parallelism was not a foregone conclusion given that mammalian visual sensory transducer rhodopsin and archaeal proton-pumping BR are found in anciently diverged organisms that differ greatly in membrane composition, architecture, metabolism, and environment.

77 Eubacterial rhodopsins have been known only since Sargasso Sea metagenomics
78 efforts uncovered proton-pumping proteorhodopsins in marine bacteria in 2000 (21),
79 followed by identification of opsin gene sequences in highly abundant nano-actinobacteria
80 in fresh water (22). Like BR, these bacterial retinylidene opsins harness photon energy to
81 pump protons across the membrane (23–25). Yet, notably, not all opsin-encoding bacteria
82 carry genes for the complete enzymatic pathway to synthesize the retinal chromophore(23,
83 24). While retinal may be scavenged in some natural environments (26–28), the incomplete
84 pathway nonetheless led us to hypothesize that ActR may moonlight (29) and exhibit a
85 second, retinal-independent function. Given that *actR* transcript levels in the natural
86 environment are extremely high (23, 30), implying abundant protein levels, this function
87 could be related to membrane structure and stability, echoing the fact that BR makes up 75%
88 of the dry weight of *Halobacterium salinarum* purple membranes (31). Alternatively, given
89 that bovine visual opsin and BR are identified scramblases (17, 20), we hypothesized that
90 ActR and other bacterial opsins would also be phospholipid scramblases. This idea was
91 bolstered by recent preliminary evidence of a Gram-negative bacterial proteorhodopsin
92 (ptqPR) from *Psychroflexus torquis* acting as a scramblase (32).

93 We now show that ActR catalyzes interchange of phospholipid between bilayer
94 leaflets. The dual ActR functions of proton pump (23) and scramblase emphasize the
95 versatility of photoreceptor function and may provide a molecular connection between
96 photoheterotrophy and membrane biogenesis.

97

98 **Results**

99 *ActR is produced in large quantities in an in vitro transcription/translation system*

100 We synthesized ActR (*Nanopelagicus ca*. genome sequence L06) in a wheat-term
101 extract translation system (33) with the inclusion of retinal in the translation reaction.
102 Purification by nickel affinity and size exclusion yielded a single ActR protein band, migrating
103 more rapidly (<25kDa) than expected from its ~29kDa molecular weight, and co-purifying
104 with a triplet identified by mass spectrometry as chaperones from the wheat germ extract
105 (Figure 1A). The protein was highly colored (Figure 1B) with peak absorbance at 544 nm—

106 characteristic of a bacterial rhodopsin with Leucine at the tuning position, and in agreement
107 with our previous observations for bacterially produced ActR (23, 34) (Figure 1C). Purity and
108 homogeneity of ActR was further demonstrated by our ability to crystallize it using a cubic
109 lipidic phase (Figure 1B, bottom panel).
110
111 *ActR facilitates transbilayer phospholipid transport*
112 To determine the scramblase activity of ActR we used standard fluorescence-based
113 assays (Figures 1D,E) in which proteins are reconstituted into large unilamellar vesicles
114 containing a trace amount of a fluorescent phospholipid reporter, *e.g.* 4-Nitro-2,1,3-
115 benzoxadiazole (NBD-PC) (17, 20, 35). To assay scrambling, the vesicles are interrogated
116 with topological probes – the dianion dithionite (Figure 1D), which reacts with the NBD
117 fluorophore to eliminate its fluorescence, and fatty acid-free BSA (Figure 1E) which captures
118 NBD-PC molecules that desorb from the vesicle surface, resulting in partial fluorescence
119 quenching.
120 Treatment of protein-free vesicles with dithionite is expected to result in ~50%
121 fluorescence loss as NBD-PC molecules in the outer leaflet of the vesicles are modified
122 whereas those in the inner leaflet are protected (Figure 1D, top row). This is what is
123 experimentally observed (Figure 1F, trace labeled 'empty' plateaus at 53%). However, when
124 the vesicles contain an active scramblase, rapid exchange of NBD-PC between the inner
125 and outer leaflets of the vesicle results in total loss of fluorescence as the entire
126 complement of NBD-PC becomes exposed to dithionite (Figure 1D, bottom row). We
127 reconstituted two different amounts of cell-free produced ActR via detergent-destabilization
128 of preformed liposomes. We also reconstituted bovine opsin (BO) as a positive control. As
129 shown in Figure 1F, dithionite treatment of ActR proteoliposomes (ActR-5, ActR-15) showed
130 a greater loss of fluorescence than seen with empty vesicles (L), indicating that ActR has
131 scramblase activity. Addition of hydroxylamine, which disrupts the Schiff's base linkage to
132 retinal, has no impact on scrambling activity (data not shown).
133 The reconstitutions were done at a protein:phospholipid ratio of ~5 μg/μmol (ActR-5
134 and BO-5) or ~15 μg/μmol (ActR-15). As ActR is smaller than BO (~29 kDa vs ~40 kDa), it

135 would be expected to functionalize at least as many vesicles as BO when reconstituted at
136 ~5 μg/μmol. Yet, the data show that the extent of fluorescence reduction is not as great for
137 ActR-5 (73%) as for BO-5 (91%) when the proteins are similarly reconstituted (Figure 1F).
138 Even when 3x more ActR was reconstituted (ActR-15, Figure 1F), the extent of reduction was
139 ~84%. A possible explanation for the lower efficiency with which ActR reconstitutes is that
140 the protein multimerizes *en route* to reconstitution and consequently populates fewer
141 vesicles with functional scramblases.

142 The fluorescence decay traces for ActR and BO-containing vesicles are well fit with a
143 double-exponential decay function which represents a convolution of the dithionite
144 reduction reaction rate ($t_{1/2}$ ~12 s) and a slower scrambling rate. For BO-5, the slow phase
145 has $t_{1/2}$ ~40s, whereas for ActR-5 and ActR-15, the $t_{1/2}$ values are ~400 and ~180 s,
146 respectively. These values suggest that ActR-mediated scrambling is somewhat slower
147 under these experimental conditions than that observed for BO.

148 To complement data generated using diothionite, we next used BSA as a topological
149 probe. For empty vesicles, ~30% fluorescence loss is expected, as NBD-PC from the outer
150 leaflet of the vesicles is quantitatively captured by BSA (Figure 1E, top row). When bound to
151 BSA, the quantum efficiency of NBD-PC is ~60% lower than when the lipid is in the
152 membrane (8, 36). For scramblase-equipped vesicles, transbilayer exchange of NBD-PC
153 enables all NBD-PC molecules to be captured by BSA, resulting in ~60% expected
154 fluorescence loss. Figure 1G shows greater fluorescence loss in ActR-containing vesicles
155 compared with empty vesicles, consistent with their scramblase activity. As with the
156 dithionite assay, greater fluorescence reduction was seen with ActR-15 than with ActR-5,
157 and BO-5 vesicles showed close to the maximum expected fluorescence loss.

158

159 *Scramblase activity of ActR purified from E. coli*

160 As an orthogonal means to isolate ActR, and to avoid the co-purification of wheat germ
161 chaperones, we overexpressed the same ActR sequence in *E. coli*, induced expression and
162 added retinal concomitantly, and purified the protein using metal affinity and gel filtration
163 chromatographies. SDS-PAGE analysis revealed a single band running at the expected size

164 for an ActR monomer (Figure 1H), with a characteristic purple color (Figure 1I) with maximum
165 absorbance at 544 nm (Figure 1J). On reconstitution into unilamellar vesicles, the
166 bacterially-produced protein also showed robust phospholipid scramblase activity,
167 measured using the dithionite modification of NBD (Figure 1D, 1K). Thus, whether produced
168 in a cell-free system or expressed in *E. coli*, ActR demonstrates scramblase activity.
169
170 *ActR oligomeric state observed by EM*
171 Microbial opsins have been observed in a range of oligomeric states (37–39),
172 including monomeric, trimeric and pentameric. Extended helices and a 3-omega motif
173 dictate the pentameric state of *Gloeobacter* rhodopsin (40). As these secondary structures
174 are also found in ActR, we expect it to be pentameric. Furthermore, ActR contains a triplet of
175 residues (H61, D95, and S20) homologous to those in *Gloeobacter* rhodopsin that are
176 important for modulating its oligomeric state at different sample pH values (40). The
177 multimer state of ActR may be important for both its light-dependent proton-pumping and
178 scramblase activities. We investigated the ActR oligomeric state at the neutral pH under
179 which the scramblase assays were carried out, using negative stain transmission electron
180 microscopy (TEM) and analytical size-exclusion chromatography. TEM images indicate a
181 heterogeneous mixture of ActR oligomers with a preference for pentamers (Figure 2A).
182
183 *Coarse Grained Molecular Dynamics Support ActR Pentamer Scramblase Activity*
184 To support our laboratory-based observations that ActR is a lipid scramblase, we
185 employed coarse-grained molecular dynamics simulations over an extended time window
186 to assess scrambling activity of ActR in three oligomeric states. Three replicates of an ActR
187 pentamer model in a dioleoylphosphatidylcholine (DOPC) membrane bilayer showed ~4
188 scrambling events/μs (Figure 2B), consistent with rates calculated for archaeal BR (20). The
189 lipid inversion rate of two positive controls (scEMC3 with ~5 events/μs and VDAC1 dimer with
190 ~8 events/μs) were consistent with results reported by Li *et al.* (41) whose computational
191 protocol we followed. In contrast, the ActR monomer, ActR trimer, and VDAC1 monomer
192 displayed negligible scrambling activity (Figure 2B).

Our model suggests that transbilayer phospholipid diffusion occurs at protomer interfaces in ActR and involves polar and aromatic residues that form a hydrophilic groove, consistent with the previously described credit card model (15). Side chains spanning the hydrophilic groove from helix 1 of one protomer and helices 3 and 4 of the adjacent protomer are highly involved (Figure 2C,D,E), as are buried water molecules (Figure 2D). Lipid translocation takes on the order of 100 ns from initial approach to complete inversion. ActR-mediated lipid scrambling demonstrates no directional bias.

The scrambling trajectory can be described in steps. First, lipids are recruited by polar residues near the bilayer surface. For example, Tyr161 and Tyr164 on helix 5 serve this role in the event depicted in Figure 2C. The phospholipid does not linger in these positions for more than a frame or two during the coarse-grained simulation, and from 20 scrambling events chosen for a deeper analysis (of total 138 observed), these residues come into play in only 1 or 2 of the events, respectively. Thus, the recruitment step is transient and many different side chains may be able to act at this step.

After this initial recruitment of the phospholipid, the heart of the scrambling mechanism takes place within the inter-subunit groove. The phosphate bead enters a lower pocket and contacts Tyr32 (75% of events) and Thr123 (95% of events) (Figure 2C,E). During this step, the lipid tails may sample an equatorial orientation relative to the bulk lipid of the membrane (Figure 2C, 411 ns & 420 ns panels). Subsequently, Phe21 (100% of 20 events) passes the DOPC from the lower to an upper pocket. Passage into and through this second water-containing cavity formed by Asn17, Tyr93 and Tyr137 (contacted in 90%, 40% and 85% of events, respectively) is slow, with variable contact times on the order of 10 ns for these three side chains (Figure 2C-F). All of these transitions can include backsliding. The upper cavity is formed by side chains from three helices at the oligomer interface; Asn17 on helix 1 of one monomer interacts with Tyr93 on helix H3 and Tyr137 of H4 from the adjacent monomer (Figure 2C,E).

Finally, an additional step involves transient contact with surface residues (for example, Gln11 and Asn220), after which the lipid diffuses into the bulk membrane.

Discussion

Moonlighting is common among identified scramblases — multiple scrambling GPCRs (39, 42) and TMEM16 (43) in eukaryotes, numerous bacterial, ER, and mitochondrial membrane insertases (41, 44), and Gram positive (this work), Gram negative (32) and archaeal rhodopsins (20) perform other functions including ion transport, protein translocation, and signal transduction. The TMEM16 family of proteins, for example, function either as chloride channels or as nonspecific ion channels/lipid scramblases. The chloride channel members of this family may have derived from a primordial scramblase and evolved chloride transport at the expense of scramblase activity (45). It appears likely that yet-to-be discovered scramblases moonlight with other functions. The ubiquitous nature of scramblase activity in diverse membrane proteins also helps explain why it has been difficult to pinpoint a unique and essential scramblase in some organisms (5).

Rhodopsins were ancient proteins found in early-Earth life forms (46, 47), suggesting these proteins could have functioned as scramblases in the earliest cells. In the modern world, microbial rhodopsins are found across Bacteria, Archaea, and even some giant viruses (48, 49), with phylogenetic evidence suggesting that this wide distribution is due, at least in part, to frequent horizontal gene transfer (50). We are not aware of any conserved sequence motifs linked to the scramblase functionality of rhodopsins across the domains of life. This lack of sequence requirement suggests that scramblase functionality relies upon relatively hydrophilic surface characteristics without selecting for specific residues. While scramblase activity is essential, the molecular surface underpinning this function appears to be under low selective pressure, possibly owing to the high rates of lipid scrambling exhibited by even rudimentary scramblases (51, 52) that may render scramblases easily evolvable.

Our simulations show that the ActR pentamer exhibits robust scrambling activity, consistent with the observation that more ActR is needed to functionalize vesicles in comparison to bovine opsin. Monomeric and trimeric forms of ActR showed nominal scrambling, which suggests that the capacity to facilitate lipid diffusion depends on the oligomeric state of the protein, and that a fully functional hydrophilic groove is only present

250 in the pentameric form. The dependence of activity on oligomerization aligns with
251 observations from other scramblases such as VDAC1, where dimerization is necessary to
252 form a translocation-competent groove (36) and BR, where trimerization generates
253 interfaces that can scramble lipids (20).

254 The structural basis for actinorhodopsin-mediated scrambling centers on a
255 hydrophilic groove formed by helices 1 and 3+4 of neighboring protomers. This pathway is
256 lined with aromatic and polar residues that interact with the charged phospholipid
257 headgroup to facilitate translocation. The orientation of the phospholipid during the
258 scrambling event supports the credit-card insertion model, where the charged phosphate
259 head group slides between helices, forming transient interactions with polar groups, and
260 reorients in plane with the bulk lipid as it rejoins the bilayer (Figure 2C,D,F). Coarse-grained
261 resolution limits the precision in which we can observe side chain orientation and hydrogen
262 bonding. However, repeated observations of lipid contacts indicate a core set of residues—
263 including Asn17, Phe21, Tyr32, and Tyr137—that play a role in the translocation
264 mechanism.

265 We have shown that $ActR_{L06}$ from *Nanopelagicus ca*. of the acI lineage of
266 actinobacteria is a phospholipid scramblase, making it the third known microbial opsin with
267 scramblase activity alongside Gram-negative bacterial PtqPR and archaeal BR. Our
268 demonstration of the robust scrambling activity of Gram-positive bacterial actinorhodopsins
269 supports the notion that phospholipid scrambling is a fundamental function of rhodopsins
270 across the domains of life. This insight provides a broad foundation for further study of the
271 scramblase/opsin duality. Particularly intriguing open questions are 1) Is there a pH
272 dependence of scrambling activity? The oligomeric state of *Gloeobacter* rhodopsin has been
273 shown to vary with pH (38) and our size exclusion chromatography mirrors these results
274 (data not shown). Decreased scramblase activity at low pH would prevent dissipation of the
275 proton gradient; low phospholipid pKa values enable a scenario where outer leaflet
276 phospholipids are protonated and subsequently deprotonated when scrambled to the inner
277 leaflet (53). Though *Nanopelagicus ca*. primarily inhabits the fresh water epilimnion, a
278 neutral pH habitat, freshwater lakes and bogs can contain low pH zones that may provide

279 environmental pressure for a pH-dependent adaptation of scramblase activity by ActR (54).
280 Perhaps this is a common mechanism for regulating bacterial rhodopsin scramblase activity
281 with consequences for energetics as well as membrane biogenesis. 2) Does the secondary
282 antennae carotenoid associated with rhodopsin in many bacterial and archaeal opsins (23,
283 55–57) have an impact on scrambling? Further elucidation of the structural roles of
284 secondary carotenoids as well as scrambling mechanisms is necessary to understand the
285 interplay, if any, between antenna association and scramblase functionality. Although
286 carotenoid association may add to thermal stability (56), our experimental and
287 computational scrambling assays were all done in the absence of the actinorhodopsin
288 carotenoid (23) and thus we can confidently say the antennae is not required for scramblase
289 activity. 3) Is the earliest role of rhodopsin scrambling or photoheterotrophy, or did these
290 activities co-evolve? Using our coarse grained molecular dynamics pipeline, we evaluated
291 the scramblase activity of an ancient opsin sequence recently determined by ancestral
292 sequence reconstruction (46). We did not observe scramblase activity (data not shown).
293 While this monomeric model has very highly conserved residues associated with
294 photoactivity, our current study concludes that scramblase activity relies more subtly on
295 appropriate alignment of amino acids with relevant properties along a protomer interface
296 than on invariant side chain identities. The study of the evolution of scramblase activity in
297 early opsins is an exciting area that warrants additional analysis.

298 **Materials and Methods**

299 *Materials*

300 16:0-18:1 PC (POPC) (1-palmitoyl-2-oleoyl-glycero-3-phosphocholine), 16:0-18:1 PG
301 (POPG) (1-palmitoyl-2-oleoyl-sn-glycero-3-phospho-(1'-rac-glycerol) (sodium salt)), 16:0-
302 06:0 NBD PC (C6-NBD-PC) (1-palmitoyl-2-{6-[(7-nitro-2-1,3-benzoxadiazol-4-
303 yl)amino]hexanoyl}-sn-glycero-3-phosphocholine) and 14:0-06:0 NBD PC ((1-myristoyl-2-
304 {6-[(7-nitro-2-1,3-benzoxadiazol-4-yl)amino]hexanoyl}-sn-glycero-3-phosphocholine) were
305 purchased as chloroform solutions from Avanti® Polar Lipids. n-Dodecyl-B-D-maltoside
306 (DDM) was purchased from VWR International. Bio-Beads SM2 Adsorbents were purchased

307 from Bio-Rad. Amberlite XAD-2 and sodium dithionite were purchased from Sigma Aldrich,
308 and fatty acid-free BSA was from EMD Millipore. Gibson Assembly® Master Mix was
309 purchased from New England BioLabs. PhusionTM High-Fidelity DNA Polymerase
310 Transcription reaction components, including S6 RNA polymerase, NTPs, RNase inhibitor,
311 and buffer were purchased from Promega Corporation. Translation reaction components,
312 including WEPRO® 8240H, Creatine Kinase, and SUB-Amix, were purchased from CellFree
313 Sciences.

314 *Plasmid Construction*

315 DNA codon-optimized for expression in *E. coli* and encoding the amino acid
316 sequence of ActR ($ActR_{L06}$ from *Nanopelagicus* ca. single-cell amplified genome L06 (acI-B))
317 (58, 23) was cloned into a pEU-C-His flexiVector, chosen for its suitability for *in vitro* protein
318 production, under the transcriptional control of the SP6 promoter (33). Insertion of the
319 coding sequence for $ActR_{L06}$ extended with a C-terminal 6x-His tag into the pEU flexiVector
320 was performed by amplifying plasmid fragments using PCR followed by Gibson Assembly
321 (59, 60). The same DNA sequence was also inserted behind the T7 promoter of a pET-28a
322 vector using Gibson Assembly for expression in *E. coli*. Amplification of DNA fragments was
323 performed using Phusion™ High-Fidelity DNA Polymerase. Gibson Assembly was performed
324 using Gibson Assembly® Master Mix. The molecular weight of the 6x-His-tagged ActR
325 monomer is 29.7 kDa, with a predicted pI of 8.64.

326 *Large Scale Cell Free ActR Production*

327 Large scale transcription and translation reactions were carried out essentially as
328 described in Aly *et al.* (33, 61) using low magnesium buffer (Cell Free Sciences) for
329 transcription. Briefly, ActR-His_6 protein was synthesized in a 12-ml 8240H wheat germ
330 extract cell-free translation system (Cell Free Sciences) at 60 OD, using 0.1% MNG-10
331 (maltose neopentyl glycol-10) with 0.02% cholesteryl hemisuccinate (CHS) buffer, and 0.1
332 mM all-trans retinal was added during the translation. ActR was purified by Ni-affinity
333 chromatography followed by size exclusion. Protein was concentrated to approximately 15

334 mg/ml in 10 mM Hepes pH 7.5, 100 mM NaCl, 0.3 mM TCEP, 0.05% DDM, 0.01% CHS and
335 stored at -80 C.

336 *ActR Expression and Purification in* E. coli

337 BL21 (DE3) *E. coli* cells were used for recombinant expression of ActR. 10 mL of an
338 overnight culture was used to inoculate 1 L of LB supplemented with 50 µg/mL kanamycin,
339 which was then incubated with shaking (37°C, 250 rpm) until the OD_{600nm} reached 0.3, at
340 which point the temperature was reduced to 22°C. At OD_{600nm} of 0.5-0.6, ActR expression
341 was induced by adding powdered IPTG to a final concentration of 0.5 mM. All-trans retinal
342 was added concomitantly to a final concentration of 9 µM from a 50 mg/mL stock solution in
343 ethanol. After 16-20 hrs of growth in the dark, the culture was centrifuged at 4,000 g for 12
344 minutes at 4°C. After a freeze-thaw cycle, cells were resuspended in lysis buffer (50 mM Tris,
345 300 mM NaCl, 5 mM $MgCl_2$, 130 µM $CaCl_2$, 1 mg/mL lysozyme, 1 mM PMSF, pH=7.40), and
346 sonicated. This and all subsequent steps were carried out at 4°C. The sample was clarified
347 at 10,000g for 20 min, after which the supernatant was centrifuged at 40,000g for 45 min to
348 pellet membranes. The membrane fraction was resuspended in 20 mL of solubilization
349 buffer (50 mM Tris, 300 mM NaCl, 5 mM $MgCl_2$, 130 µM $CaCl_2$, 10 mg/mL DDM, pH=7.40)
350 using a Potter homogenizer, and incubated with rocking in the dark for 16-20 hrs. Aggregates
351 were removed by centrifugation at 40,000g for 20 min. The supernatant (~20 mL), now
352 containing solubilized membrane proteins, was collected and flowed continuously over 5
353 mL of Ni-NTA resin at 1 mL/min for 16-20 hrs using a peristaltic pump. The Ni-NTA resin was
354 washed with >20 bed volumes of wash buffer (50 mM Tris, 300 mM NaCl, 50 mM Imidazole,
355 0.5 mg/mL DDM, pH=7.40) and ActR was eluted with wash buffer containing successively
356 higher imidazole concentrations, from 100 mM to 500 mM. ActR-containing fractions were
357 pooled, and concentrated along with DDM in a 10 kDa – cutoff spin concentrator (Millipore).
358 Samples were dialyzed against 50 mM HEPES, 150 mM NaCl, pH=7.4 and injected onto a
359 Superdex 200 Increase 10/300 GL size exclusion column pre-equilibrated with buffer
360 identical to the dialysis reservoirs supplemented with 0.5 mg/ml DDM using an ÄKTA pure™
361 chromatography system. ActR-containing fractions were pooled, concentrated to approx.

362 0.5 mg/ml and immediately used for liposome reconstitution. The overall yield was ~0.5
363 mg/L of bacterial culture.

364 *ActR Negative Stain EM*

365 ActR expressed in *E. coli* and purified through the metal affinity chromatography step
366 was kept at 4°C and used to prepare EM grids on the same day. CF200-CU grids were glow
367 discharged for 30 s at 15 mA on a Pelco easiGlow discharge system. 4 µL of sample (diluted
368 in elution buffer to 240, 80, 32, or 8 µg/mL) was applied to each grid for 1 minute before
369 blotting. Grids were washed 2x in 20 µL buffer, 2x in 20 µL 2% Uranyl acetate (UA), followed
370 by one minute incubation in 2% UA. All images were collected on a Talos L120c 120 keV
371 electron microscope using a Ceta CMOS detector at the University of Wisconsin–Madison
372 Cryo-EM Research Center.

373 *Reconstitution of ActR into liposomes*

374 Liposomes were prepared using a 9:1 (mol/mol) POPC/POPG mixture, spiked with 0.5%
375 16:0-06:0 NBD PC or 14:0-06:0 NBD PC. The lipid mixture was prepared from chloroform
376 stock solutions, dried under nitrogen or in a rotary evaporator, and then placed under
377 vacuum overnight at ambient temperature before being resuspended in buffer (50 mM
378 HEPES, 150 mM NaCl, pH 7.4) at a concentration of ~4 mg/mL. The resuspended lipids were
379 processed further and taken for ActR reconstitution using either of two methods as follows.
380 Method 1 (used for *E. coli*-produced ActR): The sample was bath sonicated for 5 min,
381 incubated at ambient temperature for 1 h, sonicated again and aliquoted for individual
382 reconstitution experiments. Each aliquot was incubated with DDM (0.5% final) at ambient
383 temperature for 1 h, rotating end-over-end. ActR was then added, and incubation continued
384 for 1 h. Reconstitution was achieved by adding washed Amberlite XAD-2 (150 mg) followed
385 by incubation at ambient temperature for 1 h with end-over-end rotation. The samples were
386 withdrawn and added to a fresh aliquot of Amberlite, followed by incubation overnight at 4°C
387 with end-over-end rotation. Following this, the samples were withdrawn and transferred to
388 tubes containing fresh Amberlite for a final incubation at ambient temperature for 1 h. The
389 resulting proteoliposomes were stored at 4°C for up to two days, diluted 1/10 in excess buffer

390 and passed through a 0.2 μm filter on a Hamilton syringe assembly to produce a narrow size
391 distribution of ActR-containing liposomes (62, 63). Method 2 (used for cell-free synthesized
392 ActR): The sample was extruded successively through 400 nm and then 200 nm filters as
393 described (36) to generate unilamellar vesicles with an average diameter of 170 nm. TX-100
394 (0.2% final) was added to destabilize the vesicles, before adding ActR. The mixture was
395 treated with one shot of washed BioBeads to remove detergent, initially at room
396 temperature and then overnight at 4°C. The resulting vesicles were assayed directly (no
397 further extrusion).

398 *Scramblase Assays*

399 Scramblase activity assays were performed as previously described (17, 20, 64, 65),
400 using vesicles diluted to 2.5 mL in buffer (50 mM HEPES, 150 mM NaCl, pH7.4). NBD
401 fluorescence (λ_{ex}=470 nm, λ_{em}=530 nm) was monitored over time in spectrofluorimeters
402 (QuantaMaster Model C-60/2000 or Horiba) equipped with a temperature-controlled
403 cuvette holder, with a magnetic stirring apparatus. After obtaining a stable fluorescence
404 signal, dithionite (from a 1M stock) or fatty acid-free BSA (from a 75 mg/ml stock) was added.
405 Addition of dithionite (final 10-20 mM) covalently modifies the fluorescent NBD moiety and
406 eliminates its fluorescence signal (66), leading to fluorescence drops of 50-100% for protein-
407 free liposomes and scramblase-active proteoliposomes, respectively. BSA (final 15 mg/ml)
408 captures and quenches NBD-PC molecules that desorb from the outer leaflet, leading to
409 fluorescence drops of ~30-60% for protein-free liposomes and scramblase-active
410 proteoliposomes, respectively (8, 66).

411 Fluorescence traces were normalized to stable fluorescence emission values prior to
412 dithionite or BSA addition, and analyzed as described (68) using mono-exponential fits for
413 protein-free liposomes and a double-exponential fit for ActR-containing samples. Analyses
414 were performed within MATLAB or PRISM, using their curve fitting functions.

415

416 **Coarse Grained Molecular Dynamics**

417 An ActR monomer structural model was generated using Chai-1 for *de novo* structure
418 prediction (69). The crystal structure of VDAC1 (RCSB: 6G6U) and bovine opsin (RCSB:

419 4A4M) were obtained from the RCSB Protein Data Bank (70). For scEMC3, missing regions in
420 the crystal structure (6WB9) were modeled using AlphaFold (71, 72). Two BR dimers were
421 tested and compared; one generated in AlphaFold and aligned to a crystal structure (4MD2)
422 and the other a vacuum-minimized crystal structure (1AT9). We found similar scramblase
423 activity in both models, and herein we present the AI-predicted model. Coarse-grained
424 molecular dynamics (CGMD) simulations were performed on a high-throughput computing
425 cluster using the HTCondor software suite and GROMACS 2022.2 (73, 74). Visual Molecular
426 Dynamics (VMD) and Tachyon were used for trajectory visualization and image rendering (75,
427 76).

428 Protein models were initially subjected to energy minimization in a vacuum until the
429 maximum force on any atom was below 100 $kJ \cdot mol^{-1} \cdot nm^{-1}$. Both the minimization and
430 production runs were conducted using a GROMACS 2022.2 container image hosted on
431 Docker Hub. Following minimization, the ActR trimer and pentamer were built by aligning the
432 monomer to a trimeric *Halobacter salinarum* BR model (1AT9) (77) and to a pentameric
433 sodium-pumping rhodopsin (KR2) from *Dokdonia eikasta* (6YC3) which was
434 crystallographically determined at 2.1 Å resolution (37). VDAC1 monomers were aligned to
435 the anti-parallel dimer RCSB structure and subsequently manually adjusted to the highly
436 scramblase-active parallel conformation described by Jahn et al. (36).

437 Proteins were embedded in a dummy membrane using the Orientation of Proteins in
438 Membranes (OPM) web server (78). The resulting protein–membrane systems were built and
439 solvated using CHARMM-GUI, then converted to coarse-grained representations using the
440 Martini 3 force field with Elastic Network Dynamics (ElNeDyn) (79–83). Each membrane
441 leaflet contained 400–500 molecules of 1,2-dioleoyl-sn-glycero-3-phosphocholine (DOPC),
442 for a total of 800–1000 lipid molecules per bilayer. Electrostatic charges in the protein were
443 counterbalanced by adding Na^+ and Cl^- ions to solution to bring the net charge to zero. Each
444 system was solvated with approximately 2×10^4 water beads.

445 To profile lipid dynamics in the presence of putative scramblases, simulations consisted of
446 energy minimization, equilibration, and a production run with randomized initial velocities.

447 Production simulations were run for 5 × 10^8 steps with a time step of 20 fs, yielding a total
448 trajectory length of 10 μs. Temperature was maintained at 310 K using a velocity-rescaling
449 (v-rescale) thermostat within an NPT ensemble. Pressure was set to 1 bar using the
450 Parrinello–Rahman barostat. Calculations were executed on a local GROMACS container
451 and using HTCondor at the UW-Madison Center for High Throughput Computing (84).

452 Systems were interrogated for scramblase activity by measuring phosphate headgroup (PO_4)
453 angles of every DOPC every 1 ns following the method described by Li *et al*.. A vector is
454 defined whose direction bisects the angle between the two vectors from head group to lipid
455 tail for each DOPC. A buffer region is defined from 55º to 125º and an event is measured if
456 the vector goes from under 55º to over 125º (or *vice versa*). Denoising was accomplished by
457 averaging angles over 50 ns windows and sampling this smoothed data every 25 ns. The
458 number of scrambling events per microsecond were averaged across all replicates.
459 Simulations for VDAC1, scEMC3, BO, and ActR trimer were run twice and all other models
460 were run three times.

461 **Acknowledgements**

462 We thank Prof. Brian Fox and Dr. Emily Beebe of the UW-Madison Transmembrane Protein
463 Center for *in vitro* production and purification of ActR, Dr. Takefumi Morizumi and Prof. Oliver
464 Ernst (University of Toronto) for a sample of bovine opsin, and Prof. Katherine Henzler-
465 Wildman, Dr. Vilius Kurauskas and Prof. Katherine McMahon for valuable expertise. We
466 thank the Landick and Kaçar labs at the University of Wisconsin–Madison for use of
467 laboratory equipment. We thank Prof. Elizabeth R. Wright, Dr. Bryan Sibert, and Alex Cotton
468 at the University of Wisconsin–Madison Cryo-EM Research Center for negative stain cryo-
469 EM services.

470

471 **Funding and Additional Information**

472 Research was supported by the USDA (WIS03052 to KTF), Einstein Foundation Visiting
473 Fellow Program (to KTF), the Human Frontier Science Program (Ref.-No: RGP009/2023 to AM)
474 and the National Science Foundation (Grant 2425586 to AM and Graduate Research

Fellowship Grant No. 2137424 to DEH). The Transmembrane Protein Center was funded by the NIH (1U54 GM094584 to Brian Fox). Some of the fluorescence data were obtained at the University of Wisconsin – Madison Biophysics Instrumentation Facility, which was established with support from the University of Wisconsin – Madison and grants BIR-9512577 (NSF) and S10 RR13790 (NIH).

482 **References**

483 1. Zhang Y-M, Rock CO. 2008. Membrane lipid homeostasis in bacteria. Nat Rev Microbiol
484 6:222–233.

485 2. Sanyal S, Menon AK. 2009. Flipping Lipids: Why an' What's the Reason for? ACS Chem
486 Biol 4:895–909.

487 3. McConnell HM, Kornberg RD. 1971. Inside-outside transitions of phospholipids in
488 vesicle membranes. Biochemistry 10:1111–1120.

489 4. Rothman JE, Kennedy EP. 1977. Rapid transmembrane movement of newly synthesized
490 phospholipids during membrane assembly. Proc Natl Acad Sci U S A 74:1821–1825.

491 5. Hrafnsdóttir S, Menon AK. 2000. Reconstitution and Partial Characterization of
492 Phospholipid Flippase Activity from Detergent Extracts of the Bacillus subtilis Cell
493 Membrane. J Bacteriol 182:4198–4206.

494 6. Hrafnsdóttir S, Nichols JW, Menon AK. 1997. Transbilayer Movement of Fluorescent
495 Phospholipids in Bacillus megaterium Membrane Vesicles. Biochemistry 36:4969–
496 4978.

497 7. Huijbregts RPH, de Kroon AIPM, de Kruijff B. 1996. Rapid transmembrane movement of
498 C6-NBD-labeled phospholipids across the inner membrane of *Escherichia coli*.
499 Biochim Biophys Acta BBA - Biomembr 1280:41–50.

500 8. Kubelt J, Menon AK, Müller P, Herrmann A. 2002. Transbilayer Movement of Fluorescent
501 Phospholipid Analogues in the Cytoplasmic Membrane of Escherichia coli.
502 Biochemistry 41:5605–5612.

503 9. Kol MA, de Kruijff B, de Kroon AIPM. 2002. Phospholipid flip-flop in biogenic
504 membranes: what is needed to connect opposite sides. Semin Cell Dev Biol 13:163–
505 170.

506 10. Pomorski TG, Menon AK. 2016. Lipid somersaults: Uncovering the mechanisms of
507 protein-mediated lipid flipping. Prog Lipid Res 64:69–84.

508 11. Luisi PL, Walde P, Oberholzer T. 1999. Lipid vesicles as possible intermediates in the
509 origin of life. Curr Opin Colloid Interface Sci 4:33–39.

510 12. Deamer DW. 1997. The first living systems: a bioenergetic perspective. Microbiol Mol
511 Biol Rev 61:239–261.

512 13. Sebinelli HG, Syska C, Čopič A, Lenoir G. 2024. Established and emerging players in
513 phospholipid scrambling: A structural perspective. Biochimie S0300-9084(24)00218–
514 9.

515 14. Wang Y, Kinoshita T. 2023. The role of lipid scramblases in regulating lipid distributions
516 at cellular membranes. Biochem Soc Trans 51:1857–1869.

517 15. Pomorski T, Menon AK. 2006. Lipid flippases and their biological functions. Cell Mol Life
518 Sci CMLS 63:2908–2921.

519 16. Sakuragi T, Nagata S. 2023. Regulation of phospholipid distribution in the lipid bilayer
520 by flippases and scramblases. Nat Rev Mol Cell Biol 24:576–596.

521 17. Menon I, Huber T, Sanyal S, Banerjee S, Barré P, Canis S, Warren JD, Hwa J, Sakmar TP,
522 Menon AK. 2011. Opsin Is a Phospholipid Flippase. Curr Biol 21:149–153.

523 18. Hessel E, Herrmann A, Müller P, Schnetkamp PPM, Hofmann K-P. 2000. The transbilayer
524 distribution of phospholipids in disc membranes is a dynamic equilibrium. Eur J
525 Biochem 267:1473–1483.

526 19. Wu G, Hubbell WL. 1993. Phospholipid asymmetry and transmembrane diffusion in
527 photoreceptor disc membranes. Biochemistry 32:879–888.

528 20. Verchère A, Ou W-L, Ploier B, Morizumi T, Goren MA, Bütikofer P, Ernst OP, Khelashvili G,
529 Menon AK. 2017. Light-independent phospholipid scramblase activity of
530 bacteriorhodopsin from Halobacterium salinarum. Sci Rep 7:9522.

531 21. Beja O, Aravind L, Koonin EV, Suzuki MT, Hadd A, Nguyen LP, Jovanovich SB, Gates CM,
532 Feldman RA, Spudich JL, Spudich EN, DeLong EF. 2000. Bacterial rhodopsin: evidence
533 for a new type of phototrophy in the sea. Science 289:1902–1906.

534 22. Sharma AK, Zhaxybayeva O, Papke RT, Doolittle WF. 2008. Actinorhodopsins:
535 proteorhodopsin-like gene sequences found predominantly in non-marine
536 environments. Environ Microbiol 10:1039–1056.

537 23. Dwulit-Smith JR, Hamilton JJ, Stevenson DM, He S, Oyserman BO, Moya-Flores F,
538 Garcia SL, Amador-Noguez D, McMahon KD, Forest KT. 2018. acI Actinobacteria
539 Assemble a Functional Actinorhodopsin with Natively Synthesized Retinal. Appl
540 Environ Microbiol 84:e01678-18.

541 24. Keffer JL, Hahn MW, Maresca JA. 2016. Characterization of an Unconventional
542 Rhodopsin from the Freshwater Actinobacterium Rhodoluna lacicola. J Bacteriol
543 197:2704–2712.

544 25. Nakamura S, Kikukawa T, Tamogami J, Kamiya M, Aizawa T, Hahn MW, Ihara K, Kamo N,
545 Demura M. 2016. Photochemical characterization of actinorhodopsin and its
546 functional existence in the natural host. Biochim Biophys Acta BBA - Bioenerg
547 1857:1900–1908.

548 26. Hirschi S, Lemmin T, Ayoub N, Kalbermatter D, Pellegata D, Ucurum Z, Gertsch J,
549 Fotiadis D. 2024. Structural insights into the mechanism and dynamics of
550 proteorhodopsin biogenesis and retinal scavenging. Nat Commun 15:6950.

551 27. Wu X, Jiang J, Hu J. 2013. Determination and occurrence of retinoids in a eutrophic lake
552 (Taihu Lake, China): cyanobacteria blooms produce teratogenic retinal. Environ Sci
553 Technol 47:807–814.

554 28. Jaffe AL, Konno M, Kawasaki Y, Kataoka C, Béjà O, Kandori H, Inoue K, Banfield JF. 2022.
555 Saccharibacteria harness light energy using type-1 rhodopsins that may rely on retinal
556 sourced from microbial hosts. ISME J 16:2056–2059.

557 29. Singh N, Bhalla N. 2020. Moonlighting Proteins. Annu Rev Genet 54:265–285.

558 30. Hamilton JJ, Garcia SL, Brown BS, Oyserman BO, Moya-Flores F, Bertilsson S,
559 Malmstrom RR, Forest KT, McMahon KD. 2017. Metabolic Network Analysis and
560 Metatranscriptomics Reveal Auxotrophies and Nutrient Sources of the Cosmopolitan
561 Freshwater Microbial Lineage acI. mSystems 2:10.1128/msystems.00091-17.

562 31. Corcelli A, Lattanzio VMT, Mascolo G, Papadia P, Fanizzi F. 2002. Lipid-protein
563 stoichiometries in a crystalline biological membrane: NMR quantitative analysis of the
564 lipid extract of the purple membrane. J Lipid Res 43:132–140.

565 32. Fang J, Zhang Y, Zhu T, Li Y. 2023. Scramblase activity of proteorhodopsin confers
566 physiological advantages to Escherichia coli in the absence of light. iScience
567 26:108551.

568 33. Aly KA, Beebe ET, Chan CH, Goren MA, Sepúlveda C, Makino S, Fox BG, Forest KT. 2013.
569 Cell-free production of integral membrane aspartic acid proteases reveals zinc-
570 dependent methyltransferase activity of the Pseudomonas aeruginosa prepilin
571 peptidase PilD. MicrobiologyOpen 2:94–104.

572 34. Mao J, Jin X, Shi M, Heidenreich D, Brown LJ, Brown RCD, Lelli M, He X, Glaubitz C.
573 2024. Molecular mechanisms and evolutionary robustness of a color switch in
574 proteorhodopsins. Sci Adv 10:eadj0384.

575 35. Ploier B, Menon AK. 2016. A Fluorescence-based Assay of Phospholipid Scramblase
576 Activity. J Vis Exp JoVE 54635.

36. Jahn H, Bartoš L, Dearden GI, Dittman JS, Holthuis JCM, Vácha R, Menon AK. 2023. Phospholipids are imported into mitochondria by VDAC, a dimeric beta barrel scramblase. Nat Commun 14:8115.

37. Kovalev K, Astashkin R, Gushchin I, Orekhov P, Volkov D, Zinovev E, Marin E, Rulev M, Alekseev A, Royant A, Carpentier P, Vaganova S, Zabelskii D, Baeken C, Sergeev I, Balandin T, Bourenkov G, Carpena X, Boer R, Maliar N, Borshchevskiy V, Büldt G, Bamberg E, Gordeliy V. 2020. Molecular mechanism of light-driven sodium pumping. Nat Commun 11:2137.

38. Morizumi T, Ou W-L, Van Eps N, Inoue K, Kandori H, Brown LS, Ernst OP. 2019. X-ray Crystallographic Structure and Oligomerization of Gloeobacter Rhodopsin. Sci Rep 9:11283.

39. Goren MA, Morizumi T, Menon I, Joseph JS, Dittman JS, Cherezov V, Stevens RC, Ernst OP, Menon AK. 2014. Constitutive phospholipid scramblase activity of a G Protein-coupled receptor*. Nat Commun 5:5115.

40. Morizumi T, Ou W-L, Van Eps N, Inoue K, Kandori H, Brown LS, Ernst OP. 2019. X-ray Crystallographic Structure and Oligomerization of Gloeobacter Rhodopsin. Sci Rep 9:11283.

41. Li D, Rocha-Roa C, Schilling MA, Reinisch KM, Vanni S. 2024. Lipid scrambling is a general feature of protein insertases. Proc Natl Acad Sci 121:e2319476121.

42. Morra G, Razavi AM, Pandey K, Weinstein H, Menon AK, Khelashvili G. 2018. Mechanisms of lipid scrambling by the G protein-coupled receptor opsin. Struct Lond Engl 1993 26:356-367.e3.

43. Lee B-C, Menon AK, Accardi A. 2016. The nhTMEM16 Scramblase Is Also a Nonselective Ion Channel. Biophys J 111:1919–1924.

44. Bartoš L, Menon AK, Vácha R. 2024. Insertases scramble lipids: Molecular simulations of MTCH2. Struct Lond Engl 1993 32:505-510.e4.

45. Kalienkova V, Clerico Mosina V, Paulino C. 2021. The Groovy TMEM16 Family: Molecular Mechanisms of Lipid Scrambling and Ion Conduction. 16. J Mol Biol 433:166941.

46. Sephus CD, Fer E, Garcia AK, Adam ZR, Schwieterman EW, Kacar B. 2022. Earliest Photic Zone Niches Probed by Ancestral Microbial Rhodopsins. Mol Biol Evol 39:msac100.

47. DasSarma S, Schwieterman EW. 2021. Early evolution of purple retinal pigments on Earth and implications for exoplanet biosignatures. Int J Astrobiol 20:241–250.

48. Bryant DA, Frigaard N-U. 2006. Prokaryotic photosynthesis and phototrophy illuminated. Trends Microbiol 14:488–496.

49. Pinhassi J, DeLong EF, Béjà O, González JM, Pedrós-Alió C. 2016. Marine Bacterial and Archaeal Ion-Pumping Rhodopsins: Genetic Diversity, Physiology, and Ecology. Microbiol Mol Biol Rev MMBR 80:929–954.

615 50. Sharma AK, Spudich JL, Doolittle WF. 2006. Microbial rhodopsins: functional versatility
616 and genetic mobility. Trends Microbiol 14:463–469.

617 51. Nakao H, Tsujii T, Saito H, Ikeda K, Nakano M. 2025. Synergistic effects of hydrophilic
618 residues in the transmembrane region on lipid scrambling activity of dimeric helices.
619 Colloids Surf B Biointerfaces 251:114612.

620 52. Nakao H, Sugimoto Y, Ikeda K, Saito H, Nakano M. 2020. Structural Feature of Lipid
621 Scrambling Model Transmembrane Peptides: Same-Side Positioning of Hydrophilic
622 Residues and Their Deeper Position. J Phys Chem Lett 11:1662–1667.

623 53. Marsh D. 2013. Handbook of Lipid Bilayers, 2nd ed. CRC Press, Boca Raton.

624 54. Rohwer RR, Kirkpatrick M, Garcia SL, Kellom M, McMahon KD, Baker BJ. 2025. Two
625 decades of bacterial ecology and evolution in a freshwater lake. Nat Microbiol 10:246–
626 257.

627 55. Balashov SP, Imasheva ES, Boichenko VA, Antón J, Wang JM, Lanyi JK. 2005.
628 Xanthorhodopsin: A Proton Pump with a Light-Harvesting Carotenoid Antenna.
629 Science 309:2061–2064.

630 56. Chuon K, Shim J, Kang K-W, Cho S-G, Hour C, Meas S, Kim J-H, Choi A, Jung K-H. 2022.
631 Carotenoid binding in Gloeobacteria rhodopsin provides insights into divergent
632 evolution of xanthorhodopsin types. Commun Biol 5:1–8.

633 57. Tzlil G, Marín MDC, Matsuzaki Y, Nag P, Itakura S, Mizuno Y, Murakoshi S, Tanaka T,
634 Larom S, Konno M, Abe-Yoshizumi R, Molina-Márquez A, Bárcenas-Pérez D, Cheel J,
635 Koblížek M, León R, Katayama K, Kandori H, Schapiro I, Shihoya W, Nureki O, Inoue K,
636 Rozenberg A, Chazan A, Béjà O. 2025. Structural insights into light harvesting by
637 antenna-containing rhodopsins in marine Asgard archaea. Nat Microbiol 10:1484–
638 1500.

639 58. Garcia SL, McMahon KD, Martinez-Garcia M, Srivastava A, Sczyrba A, Stepanauskas R,
640 Grossart HP, Woyke T, Warnecke F. 2013. Metabolic potential of a single cell belonging
641 to one of the most abundant lineages in freshwater bacterioplankton. ISME J 7:137–
642 147.

643 59. Gibson DG, Young L, Chuang R-Y, Venter JC, Hutchison CA, Smith HO. 2009. Enzymatic
644 assembly of DNA molecules up to several hundred kilobases. Nat Methods 6:343–
645 345.

646 60. Heydenreich FM, Miljuš T, Jaussi R, Benoit R, Milić D, Veprintsev DB. 2017. High-
647 throughput mutagenesis using a two-fragment PCR approach. Sci Rep 7:6787.

648 61. Beebe ET, Makino S-I, Nozawa A, Matsubara Y, Frederick RO, Primm JG, Goren MA, Fox
649 BG. 2011. Robotic large-scale application of wheat cell-free translation to structural
650 studies including membrane proteins. New Biotechnol 28:239–249.

651 62. Dearden GI, Ravishankar V, Sakata K, Menon AK, Bergdoll L. 2024. Protocol for the
652 production and reconstitution of VDAC1 for functional assays. STAR Protoc 5:103240.

653 63. Ong SGM, Chitneni M, Lee KS, Ming LC, Yuen KH. 2016. Evaluation of Extrusion
654 Technique for Nanosizing Liposomes. 4. Pharmaceutics 8:36.

655 64. Brunner JD, Schenck S, Dutzler R. 2016. Structural basis for phospholipid scrambling in
656 the TMEM16 family. Curr Opin Struct Biol 39:61–70.

657 65. Malvezzi M, Chalat M, Janjusevic R, Picollo A, Terashima H, Menon AK, Accardi A. 2013.
658 Ca2+-dependent phospholipid scrambling by a reconstituted TMEM16 ion channel.
659 Nat Commun 4:2367.

660 66. Chang Q, Gummadi SN, Menon AK. 2004. Chemical Modification Identifies Two
661 Populations of Glycerophospholipid Flippase in Rat Liver ER. Biochemistry 43:10710–
662 10718.

663 67. McIntyre JC, Sleight RG. 1991. Fluorescence assay for phospholipid membrane
664 asymmetry. Biochemistry 30:11819–11827.

665 68. Menon I, Sych T, Son Y, Morizumi T, Lee J, Ernst OP, Khelashvili G, Sezgin E, Levitz J,
666 Menon AK. 2024. A cholesterol switch controls phospholipid scrambling by G protein-
667 coupled receptors. J Biol Chem 300:105649.

668 69. Team CD, Boitreaud J, Dent J, McPartlon M, Meier J, Reis V, Rogozhonikov A, Wu K. 2024.
669 Chai-1: Decoding the molecular interactions of life. bioRxiv
670 https://doi.org/10.1101/2024.10.10.615955.

70. Razeto A, Gribbon P, Loew C. 2019. The dynamic nature of the VDAC1 channels in bilayers: human VDAC1 at 2.7 Angstrom resolution: 6g6u.

71. Jumper J, Evans R, Pritzel A, Green T, Figurnov M, Ronneberger O, Tunyasuvunakool K, Bates R, Žídek A, Potapenko A, Bridgland A, Meyer C, Kohl SAA, Ballard AJ, Cowie A, Romera-Paredes B, Nikolov S, Jain R, Adler J, Back T, Petersen S, Reiman D, Clancy E, Zielinski M, Steinegger M, Pacholska M, Berghammer T, Bodenstein S, Silver D, Vinyals O, Senior AW, Kavukcuoglu K, Kohli P, Hassabis D. 2021. Highly accurate protein structure prediction with AlphaFold. Nature 596:583–589.

72. Bai L, You Q, Feng X, Kovach A, Li H. 2020. Structure of the ER membrane complex, a transmembrane-domain insertase. Nature 584:475–478.

73. Bekker H, Berendsen HJC, Djikstra EJ, Achterop S, van Drunen R, van der Spoel D, Sijbers A, Keegstra H. 1993. Gromacs: A parallel computer for molecular dynamics simulations, p. 252–256. *In* de Groot, RA, Nadrchal, J (eds.), Physics Computing ’92. World Scientific, Singapore.

74. Thain D, Tannenbaum T, Livny M. 2005. Distributed computing in practice: the Condor experience. Concurr - Pract Exp 17:323–356.

75. Humphrey W, Dalke A, Schulten K. 1996. VMD: Visual molecular dynamics. J Mol Graph 14:33–38.

76. Stone J. 1998. An Efficient Library for Parallel Ray Tracing and Animation. Computer Science Department, University of Missouri-Rolla.

77. Kimura Y, Vassylyev DG, Miyazawa A, Kidera A, Matsushima M, Mitsuoka K, Murata K, Hirai T, Fujiyoshi Y. 1997. Surface of bacteriorhodopsin revealed by high-resolution electron crystallography. Nature 389:206–211.

78. Lomize MA, Pogozheva ID, Joo H, Mosberg HI, Lomize AL. 2012. OPM database and PPM web server: resources for positioning of proteins in membranes. Nucleic Acids Res 40:D370-376.

79. Jo S, Kim T, Iyer VG, Im W. 2008. CHARMM-GUI: A web-based graphical user interface for CHARMM. J Comput Chem 29:1859–1865.

80. Brooks BR, Brooks III CL, Mackerell Jr. AD, Nilsson L, Petrella RJ, Roux B, Won Y, Archontis G, Bartels C, Boresch S, Caflisch A, Caves L, Cui Q, Dinner AR, Feig M, Fischer S, Gao J, Hodoscek M, Im W, Kuczera K, Lazaridis T, Ma J, Ovchinnikov V, Paci E, Pastor RW, Post CB, Pu JZ, Schaefer M, Tidor B, Venable RM, Woodcock HL, Wu X, Yang W, York DM, Karplus M. 2009. CHARMM: The biomolecular simulation program. J Comput Chem 30:1545–1614.

81. Lee J, Cheng X, Swails JM, Yeom MS, Eastman PK, Lemkul JA, Wei S, Buckner J, Jeong JC, Qi Y, Jo S, Pande VS, Case DA, Brooks CLI, MacKerell ADJr, Klauda JB, Im W. 2016. CHARMM-GUI Input Generator for NAMD, GROMACS, AMBER, OpenMM, and CHARMM/OpenMM Simulations Using the CHARMM36 Additive Force Field. J Chem Theory Comput 12:405–413.

82. Qi Y, Ingólfsson HI, Cheng X, Lee J, Marrink SJ, Im W. 2015. CHARMM-GUI Martini Maker for Coarse-Grained Simulations with the Martini Force Field. J Chem Theory Comput 11:4486–4494.

83. Hsu P-C, Bruininks BMH, Jefferies D, Cesar Telles de Souza P, Lee J, Patel DS, Marrink SJ, Qi Y, Khalid S, Im W. 2017. CHARMM-GUI Martini Maker for modeling and simulation of complex bacterial membranes with lipopolysaccharides. J Comput Chem 38:2354–2363.

84. Center for High Throughput Computing. (2006). doi:10.21231/GNT1-HW21

719 **Figure Legends**

720 **Figure 1.** acI-B (*Nanopelagicus* ca.) $ActR_{L06}$ expressed in a cell free system or in *E. coli* is a
721 phospholipid scramblase

722 (A/H) SDS-PAGE analysis of affinity-purified (A) cell free- or (H) *E. coli*-produced $ActR_{L06}$
723 following size-exclusion chromatography. (B/I) Image of (B) cell free- or (I) *E. coli*-produced
724 $ActR_{L06}$ showing strong reddish color. (C/J) Absorbance spectrum of (C) cell free- or (G) *E.*
725 *coli*-produced $ActR_{L06}$. Note maximum absorbance at 543 nm.

726 (D) Protein free liposomes (L) and scramblase-containing proteoliposomes are shown. The
727 vesicles are prepared with a trace quantity of NBD-PC distributed equally between inner and
728 outer leaflets. Upon addition of dithionite, the nitro group in NBD-PC is covalently modified
729 to an amino group and the resulting ABD-PC is non-fluorescent. Liposomes retain
730 fluorescence signal from NBD-PC in the inner leaflet as dithionite cannot enter the vesicles;
731 for scramblase containing-proteoliposomes, lipids in the inner and outer leaflets exchange
732 and fluorescence emission decays further as NBD-PC molecules in the inner leaflet reach
733 the outer leaflet where they are modified by dithionite.

734 E) As in D), except that fatty-acid free BSA is used as a topological probe. NBD-PC molecules
735 that desorb from the outer leaflet of the outer membrane are captured BSA. In complex with
736 BSA, NBD-PC fluorescence is ~60% lower than when the lipid is in the membrane.

737 F/G/K) Normalized time course scramblase assay data for (F) cell free- or (K) *E. coli*-produced
738 $ActR_{L06}$. Dithionite or BSA is added at t=0 s. Error bars in panel G represent standard
739 deviation of duplicate measurements. Proteoliposomes were generated using ActR or
740 bovine opsin (BO) at different protein/phospholipid ratios (units of ug/umol) as indicated on
741 the trace lables, e.g. ActR-5 and ActR-15 represent samples with protein/phospholipid ratios
742 of 4 and 15, respectively. NBD fluorescence decays according to lipid vesicle contents.

743 **Figure 2**. ActR is a Pentamer that Facilitates Scrambling as Assessed Computationally

A) Array of four representative negative stain electron microscopy images of ActR at pH=8.0, and superposition of representative ActR TEM image over predicted ActR pentameric structure.

B) CGMD scramblase events/second accompanied by structural images. The upper right inset shows the angles (in orange) in which rotations were not counted as scrambling events.

C) GCMD scramblase “flip book” images of one DOPC moving through cleft and re-orienting lipid tails. Those beads which were within 5 Å of the phosphate bead in any frame are shown in green, PO4 bead is red, and lipid tail beads are blue.

D) One snapshot from the trajectory represented in part C is shown with beads from each opsin monomer shaded differently to highlight the inter-protomer location of the groove.

E) Ribbon diagram of the two adjacent protomers that form the scrambling groove, with critical side chains shown and labeled.

F) Z-axis height above or below the center of the membrane for the PO4 bead as a function of time during passage through cleft. Dwell times for Y32, F21, and Y137 depicted as colored bars.

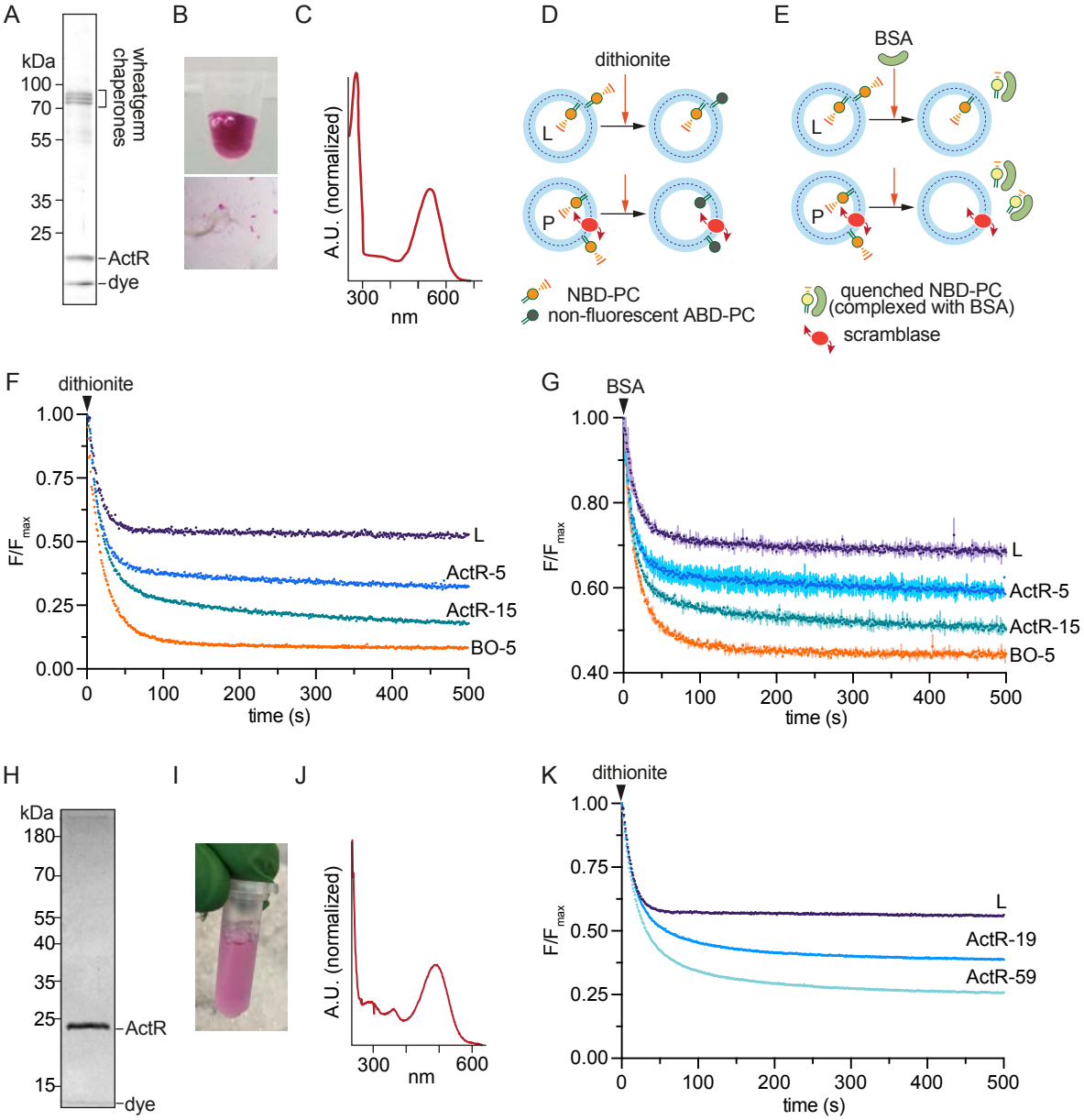

Maschmann et al., Fig 1

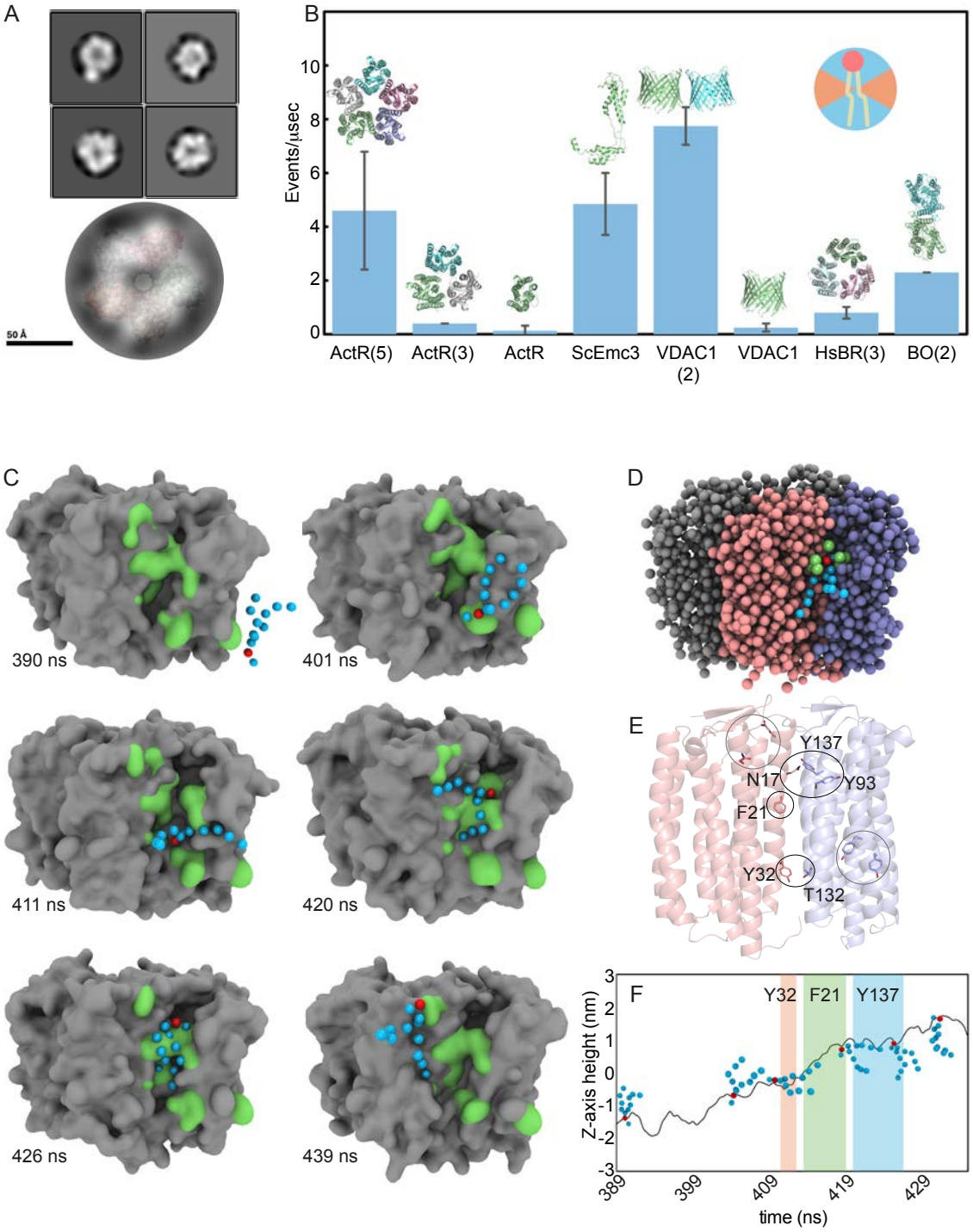

Maschmann et al., Fig 2